Phage anti-CBASS protein simultaneously sequesters cyclic trinucleotides and dinucleotides

Xueli Cao[1,11], Yu Xiao[2,11], Erin Huiting[3,11], Xujun Cao[4,5,6,7], Dong Li[1], Jie Ren[8], Linlin Guan[1], Yu Wang[1], Lingyin Li[5,6,7], Joseph Bondy-Denomy[3,9,10,*], Yue Feng[1,12,*]

[1]Beijing Advanced Innovation Center for Soft Matter Science and Engineering, State Key Laboratory of Chemical Resource Engineering, College of Life Science and Technology, Beijing University of Chemical Technology, Beijing 100029, China

[2]Ministry of Education Key Laboratory of Protein Science, Beijing Advanced Innovation Center for Structural Biology, Beijing Frontier Research Center for Biological Structure, School of Life Sciences, Tsinghua University, Tsinghua-Peking Center for Life Sciences, Beijing 100084, China

[3]Department of Microbiology and Immunology, University of California, San Francisco, San Francisco, CA, 94158, USA

[4]Department of Chemistry, Stanford University, Stanford, CA, 94305, USA

[5]Department of Biochemistry, Stanford University, Stanford, CA, 94305, USA

[6]Sarafan ChEM-H Institute, Stanford University, Stanford, CA, 94305, USA

[7]Arc Institute, Palo Alto, CA, 94304, USA

[8]State Key Laboratory for Biology of Plant Diseases and Insect Pests, Ministry of Agriculture, Institute of Plant Protection, Chinese Academy of Agricultural Sciences, Beijing 100081, China

[9]Quantitative Biosciences Institute, University of California, San Francisco, San Francisco, CA 94158, USA

[10]Innovative Genomics Institute, Berkeley, CA 94720, USA

[11]Authors contributed equally

[12]Lead Contact

*Correspondence: Joseph.Bondy-Denomy@ucsf.edu, fengyue@mail.buct.edu.cn

Summary

CBASS is a common anti-phage immune system that uses cyclic oligonucleotide signals to activate effectors and limit phage replication. In turn, phages encode anti-CBASS (Acb) proteins. We recently uncovered a widespread phage anti-CBASS protein Acb2 that acts as a "sponge" by forming a hexamer complex with three cGAMP molecules. Here, we identified that Acb2 binds and sequesters many CBASS and cGAS-produced cyclic dinucleotides *in vitro* and inhibits cGAMP-mediated STING activity in human cells. Surprisingly, Acb2 also binds CBASS cyclic trinucleotides 3'3'3'-cyclic AMP-AMP-AMP (cA$_3$) and 3'3'3'-cAAG with high affinity. Structural characterization identified a distinct binding pocket within the Acb2 hexamer that binds two cyclic trinucleotide molecules and another binding pocket that binds to cyclic dinucleotides. Binding in one pocket does not allosterically alter the other, such that one Acb2 hexamer can simultaneously bind two cyclic trinucleotides and three cyclic dinucleotides. Phage-encoded Acb2 provides protection from Type III-C CBASS that uses cA$_3$ signaling molecules *in vivo* and blocks cA$_3$-mediated activation of the endonuclease effector *in vitro*. Altogether, Acb2 sequesters nearly all known CBASS signaling molecules through two distinct binding pockets and therefore serves as a broad-spectrum inhibitor of cGAS-based immunity.

Introduction

Anti-viral immune pathways across all kingdoms of life sense and respond to viral infection. Cyclic GMP-AMP synthase (cGAS) is an evolutionarily conserved enzyme that performs a pivotal role in innate immunity against viruses (Li et al., 2013). In mammalian cells, cGAS binds viral DNA and is activated to produce 2',3'-cyclic GMP-AMP (2',3'-cGAMP) dinucleotides, which binds to and activates the STING (stimulator of interferon genes) effector protein to initiate a potent interferon response (Burdette et al., 2011; Ishikawa and Barber, 2008). In bacteria, cGAS-like enzymes named cGAS/DncV-like nucleotidyltransferases (CD-NTases) have been identified and enzymatically characterized (Burroughs et al., 2015; Davies et al., 2012; Whiteley et al., 2019). CD-NTases have been classified into 8 enzymatic clades and at least 12 cyclic di- and tri-nucleotide products have been identified (Burroughs et al., 2015; Davies et al., 2012; Duncan-Lowey et al., 2021; Fatma et al., 2021; Millman et al., 2020; Whiteley et al., 2019).   During phage infection, these enzymes are activated and produce cyclic oligonucleotides that bind to and activate a downstream effector protein. The activated effector proteins are proposed to induce premature cell death through various mechanisms, including membrane impairment (Cohen et al., 2019; Duncan-Lowey et al., 2021), DNA degradation (Fatma et al., 2021; Lau et al., 2020; Lowey et al., 2020), NAD^+ depletion (Ko et al., 2022; Morehouse et al., 2022), amongst others. This anti-phage strategy was named cyclic-oligonucleotide-based anti-phage signaling system (CBASS).

As a countermeasure to CBASS immunity, phages encode anti-CBASS proteins. Acb1 degrades the cyclic nucleotide messengers to inhibit CBASS (Hobbs et al., 2022) and Acb2 is a cyclic dinucleotide (CDN) sponge (Huiting et al., 2023; Jenson et al., 2023). Interestingly, Acb2 also binds to a variety of other CDNs: 2',3'-cGAMP and 3',3'-cUU/UA/UG/AA with varying affinities. Structures of Acb2 from *P. aeruginosa* phage PaMx33 and from *E. coli* phage T4 in complex with 3',3'-cGAMP showed that Acb2 forms an interlocked hexamer and binds to three cyclic dinucleotides, each with a binding pocket located in one Acb2 dimer within the hexamer (Huiting et al., 2023; Jenson et al., 2023). However, it remains unknown whether Acb2 binds to cyclic oligonucleotides that are utilized in Pycsar, CBASS and Type III CRISPR-Cas signaling systems (Molina et al., 2020; Tal et al., 2021; van Beljouw et al., 2022). Here, we find that Acb2 not only binds to and sequesters a broad spectrum of cyclic dinucleotides, but it also binds to cyclic trinucleotides 3'3'3'-cyclic AMP-AMP-AMP (cA_3 hereafter)

88 and 3'3'3'-cAAG (cAAG) with an order of magnitude higher affinity. CBASS systems commonly use

89 these cyclic trinucleotide signals, as do some Type III CRISPR-Cas systems (Mayo-Muñoz et al., 2022).

90 Structural characterization identified that one Acb2 hexamer binds two cyclic trinucleotides within

91 binding pockets that are different from those binding cyclic dinucleotides. A co-structure of Acb2

92 bound to cA_3 and 3',3'-cGAMP at the same time is presented, as are mutants that independently disrupt

93 the different binding sites. Phage-encoded Acb2 effectively protects phage when infecting cells

94 simultaneously expressing cA_3 and cGAMP CBASS systems. Together, this work identifies two

95 distinct cyclic oligonucleotide binding sites on Acb2 and demonstrates that Acb2 is an effective, broad-

96 spectrum inhibitor of CBASS and cGAS-STING signaling pathways.

97

98 **Results**

99 **Acb2 sequesters diverse cyclic dinucleotides and is active in human cells**

100 To understand the selectively of the newly identified Acb2 protein fold, we comprehensively tested an

101 array of cyclic oligonucleotides that Acb2 may bind to. Previous work revealed that Acb2 binds to

102 3',3'-cGAMP, 2',3'-cGAMP and 3',3'-cUU/UA/UG/AA, but not 3',3'-cGG (Huiting et al., 2023)

103 (Figure S1A-B). The study of Acb1 showed that, among cyclic dinucleotides, it does not cleave 3',2'-

104 cGAMP or 3',3'-cGG/cUU (Hobbs et al., 2022).. In this current study, we first tested Acb2 binding of

105 3',2'-cGAMP, which was recently identified as a signaling molecule for both CBASS and cGAS-like

106 enzymes in eukaryotes (Fatma et al., 2021; Slavik et al., 2021). Interestingly, a native gel assay showed

107 a significant shift of the Acb2 protein upon adding 3',2'-cGAMP (Figure 1A), and isothermal

108 calorimetry (ITC) experiments verified that Acb2 binds to 3',2'-cGAMP with a K_D of ~297.7 nM

109 (Figures 1B and S2). Next, we solved the structure of Acb2 complexed with 3',2'-cGAMP (2.33 Å),

110 in which 3',2'-cGAMP showed a similar binding mode as 3',3'-cGAMP and c-di-AMP (Figures 1C-

111 E and Table 1). Specifically, these dinucleotide molecules are bound by the N-terminal domains of the

112 two interacting Acb2 protomers, and the π-π stacking from Y11 residue and salt bridges from K26

113 residue of both protomers further stabilizes this interaction (Figures 1D-E). The structure of Acb2

114 complexed with another cGAMP isomer, 2',3'-cGAMP, solved at 2.24 Å resolution further confirmed

115 this mode of binding (Figure 1E and Table 1). Since 3',2'-cGAMP and 2',3'-cGAMP are ligands used

116 in eukaryotic cGAS-STING immunity, we also tested whether Acb2 can antagonize cGAS-STING

117 signaling pathway in human cells. The results showed that upon expression of WT Acb2, interferon

118 (IFN) signaling mediated by 2',3'-cGAMP is significantly reduced while Y11A and K26A Acb2

119 mutants were less active (Figure 1F). Consistent with these data, native gel assays showed that Y11A

120 and K26A mutations abrogated 2',3'-cGAMP binding (Figure S1C). Taken together, our data

121 demonstrates that Acb2 harbors a binding pocket that is well suited for many cyclic dinucleotides.

122
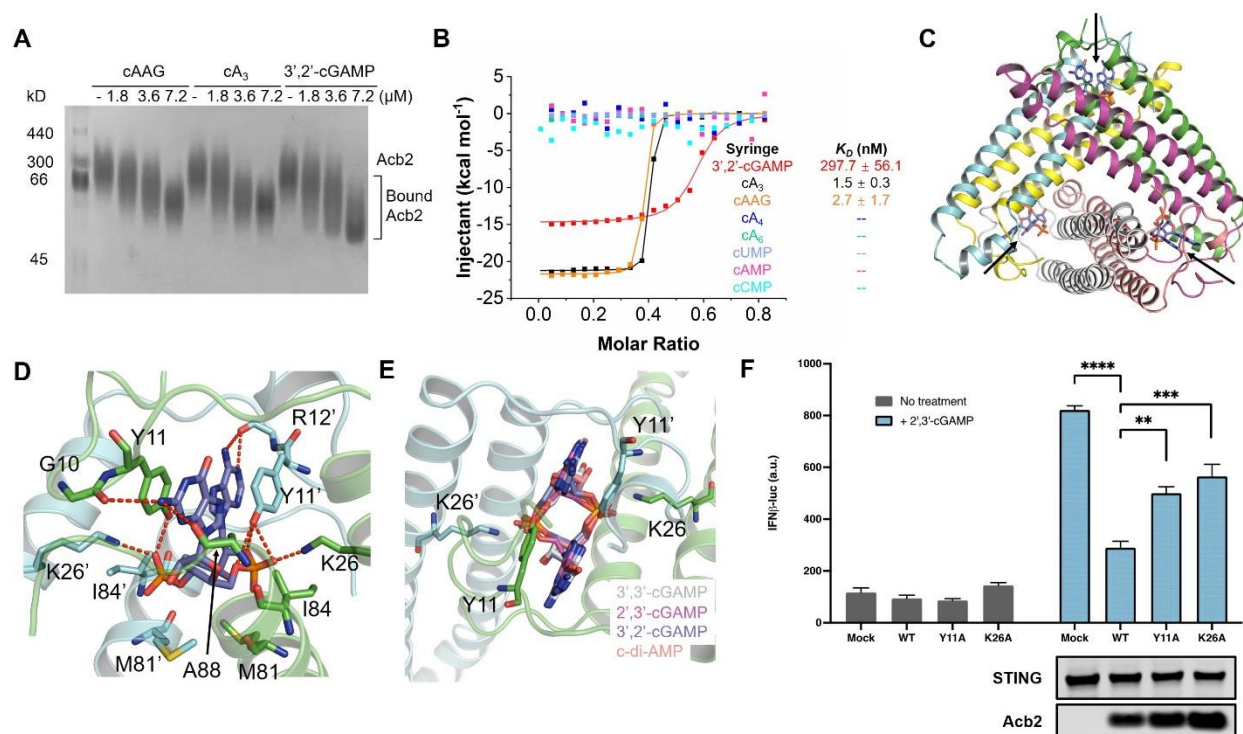
123 **Figure 1. PaMx33 Acb2 also binds cyclic trinucleotides and 3', 2'-cGAMP**

124 (A) Native PAGE showed the binding of PaMx33-Acb2 to cyclic oligonucleotides.

125 (B) ITC assays to test binding of cyclic nucleotides to PaMx33-Acb2. Representative binding curves

126 and binding affinities are shown. The K_D values are mean ± s.d. (n=3). Raw data for these curves are

127 shown in Figure S2.

128 (C) Overall structure of Acb2 complexed with 3',2'-cGAMP, which are indicated by arrows.

129 (D) Detailed binding between Acb2 and 3',2'-cGAMP. Residues involved in 3',2'-cGAMP binding are

130 shown as sticks. Red dashed lines represent polar interactions.

131 (E) Structural alignment among 3',2'-cGAMP, 2',3'-cGAMP, 3',3'-cGAMP and c-di-AMP bound

132 Acb2, highlighting the binding pocket of cyclic dinucleotides.

133 (F) 293T-Dual cells were transfected with hSTING and Acb2 or its mutants, then treated with 2',3'-

134 cGAMP. STING activation was read as luciferase signal controlled by an interferon promoter.

135

136 **Acb2 sequesters cyclic trinucleotides with higher affinity than cyclic dinucleotides**

137   Based on the binding pocket of Acb2, we hypothesized that Acb2 may not bind cyclic mononucleotides

138   or oligonucleotides, such as cA_3, cA_4 or cA_6, due to potential steric clash caused by the nucleotides.

139   Of note, cA_3 and cAAG are major products of the CD-NTase enzymes involved in CBASS whereas

140   cA_4 is only a minor product of a single CD-NTase (Lowey et al., 2020). cA_6 has not been identified as

141   a product of any known CD-NTases. However, all three cyclic oligoadenylates are known products

142   involved in Type III CRISPR-Cas anti-phage immunity (Athukoralage and White, 2022). A native gel

143   assay showed that the Acb2 protein does not shift upon adding cA_4 or cA_6 molecules (Figures S1A-B).

144   Furthermore, both native gel and ITC assays showed that Acb2 does not bind to cUMP, cCMP or cAMP

145   (Figures S1-2 and 1B). However, the native gel assay revealed a significant shift of the Acb2 protein

146   upon adding cA_3 or cAAG. ITC experiments revealed that Acb2 binds to cA_3 and cAAG with a K_D of

147   ~1.5 and ~2.7 nM (Figures 1B and S2), respectively, which is more than an order of magnitude stronger

148   than Acb2 binding to 3',3'-cGAMP (K_D of ~87 nM) (Huiting et al., 2023). To determine whether Acb2

149   sequesters or cleaves the cyclic trinucleotide molecules, high-performance liquid chromatography

150   (HPLC) revealed that incubating Acb2 with cA_3 depletes any detectable molecules, and following

151   proteolysis of Acb2, cA_3 is released back into the buffer unmodified (Figure 2A). Collectively, these

152   results demonstrate that Acb2 binds to and sequesters cyclic trinucleotides commonly used in CBASS

153   immunity with a significantly higher affinity than cyclic dinucleotides.

154

155   **Acb2 binds cyclic trinucleotides and dinucleotides with different binding sites**

156   The binding of cyclic trinucleotides was unexpected because the Acb2 binding pocket appears well

157   suited for only cyclic dinucleotides. To understand how Acb2 interacts with cyclic trinucleotides, we

158   determined the crystal structures of Acb2 in complex with cA_3 (2.26 Å) or cAAG (2.10 Å) (Table 1).

159   Surprisingly, the structures showed that one Acb2 hexamer binds two cyclic trinucleotides with two

160   distinct binding pockets that are far from the three pockets for the cyclic dinucleotide binding (Figures

161   2B and S3A-B). Each binding site of the cyclic trinucleotides is formed by three Acb2 protomers in a

162   three-fold symmetry and the two binding sites are opposite each other (Figure 2B). In turn, each of the

163   two protomers that together bind a cyclic dinucleotide is involved in binding to one out of the two

164   cyclic trinucleotides, respectively (Figure S3A). Correspondingly, each of the three protomers that

165   together bind a cyclic trinucleotide is involved in binding to one out of the three cyclic dinucleotides,

166   respectively (Figure S3B).
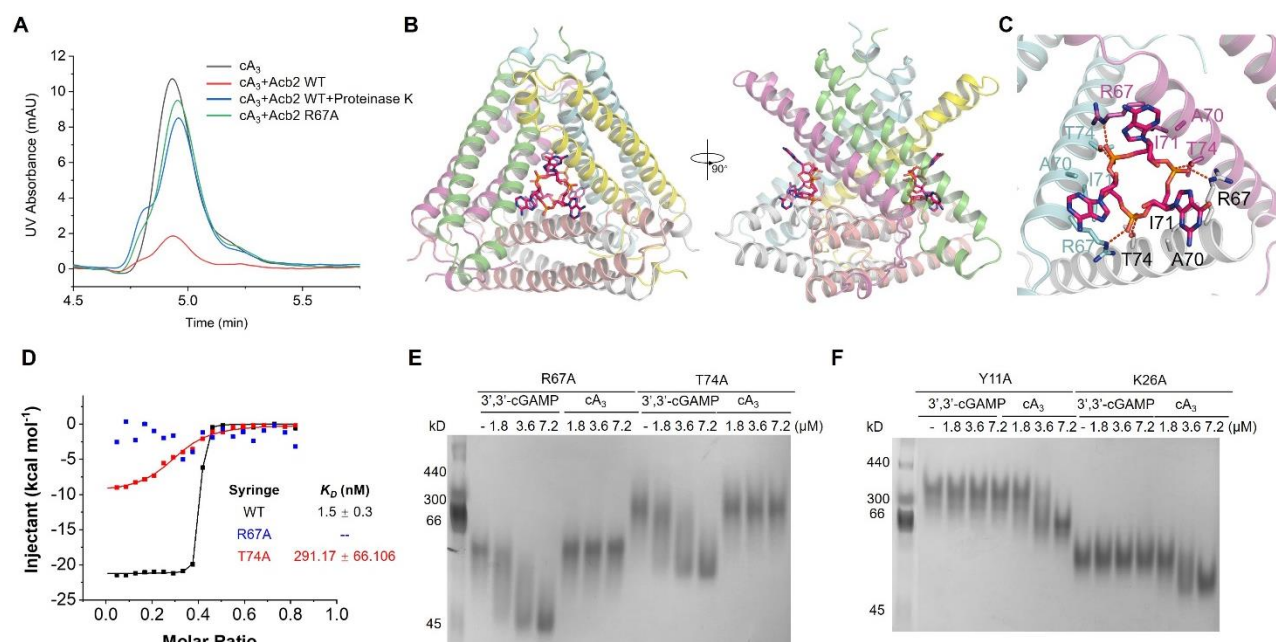
Figure 2. Acb2 binds to cyclic trinucleotides with binding sites different from those of cyclic dinucleotides

(A) The ability of PaMx33-Acb2 to bind and release cA_3 when treated with proteinase K was analyzed by HPLC. cA_3 standard was used as a control. The remaining cA_3 after incubation with PaMx33-Acb2 was tested.

(B) Overall structure of Acb2 complexed with cAAG, which are shown as sticks. Two views are shown.

(C) Detailed binding between Acb2 and cAAG. Residues involved in cAAG binding are shown as sticks. Red dashed lines represent polar interactions.

(D) ITC assays to test the binding of cA_3 to PaMx33-Acb2 mutants. Representative binding curves and binding affinities are shown. The K_D values are mean ± s.d (n = 3). Raw data for these curves are shown in Figure S2.

(E-F) Native PAGE showed the binding of PaMx33 Acb2 mutants to cyclic oligonucleotides.

The cyclic trinucleotide is bound mainly through its three phosphate groups, each of which is coordinated by R67 of one protomer and T74 of another protomer through hydrogen bonds (Figure 2C). Moreover, the cyclic trinucleotide is also stabilized by hydrophobic interactions from R67, A70 an I71 from each of the three protomers (Figure 2C). Consistent with this analysis, the Acb2 T74A mutant displayed a significantly decreased binding affinity to cA_3 (K_D of ~291 nM), and the Acb2 R67A mutant abolished Acb2 binding of cA_3 *in vitro* (Figures 2D and S2). To confirm that the binding

187   sites of the cyclic trinucleotides and dinucleotides in Acb2 are independent of each other, we tested the

188   binding of 3',3'-cGAMP with the T74A or R67A Acb2 mutant proteins. A native gel assay showed

189   similar shifts of the two Acb2 mutants as WT Acb2 upon adding 3',3'-cGAMP (Figure 2E), suggesting

190   that the binding to 3',3'-cGAMP is not affected by the two mutations. In turn, we tested the binding of

191   cA_3 with Y11A and K26A Acb2 mutants, which lose their binding to 3',3'-cGAMP   (Huiting et al.,

192   2023). The native gel results showed a significant shift of Y11A and K26A mutant proteins upon adding

193   cA_3 (Figure 2F). Taken together, these data collectively show that one Acb2 hexamer binds two cyclic

194   trinucleotides through two pockets independent of those that bind cyclic dinucleotides.

195

196   Structural alignment between apo Acb2 and its complexes with cyclic trinucleotides showed that the

197   binding of cyclic trinucleotides does not induce a conformational change of Acb2, with a root mean

198   square deviation (RMSD) of 0.224 and 0.261 Å (Cα atoms) for Acb2-cA_3 and Acb2-cAAG compared

199   to the apo Acb2, respectively (Figure S3C). Therefore, we co-crystallized Acb2 with both cA_3 and

200   3',3'-cGAMP and then solved its crystal structure at a resolution of 2.76 Å (Table 1). The structure

201   clearly showed that Acb2 binds to two cA_3 and three 3',3'-cGAMP molecules simultaneously (Figures

202   3A-C). Structural alignment between Acb2-cA_3-3',3'-cGAMP and apo Acb2 also showed little

203   conformational changes with an RMSD of 0.298 Å for Cα atoms (Figure S3D).
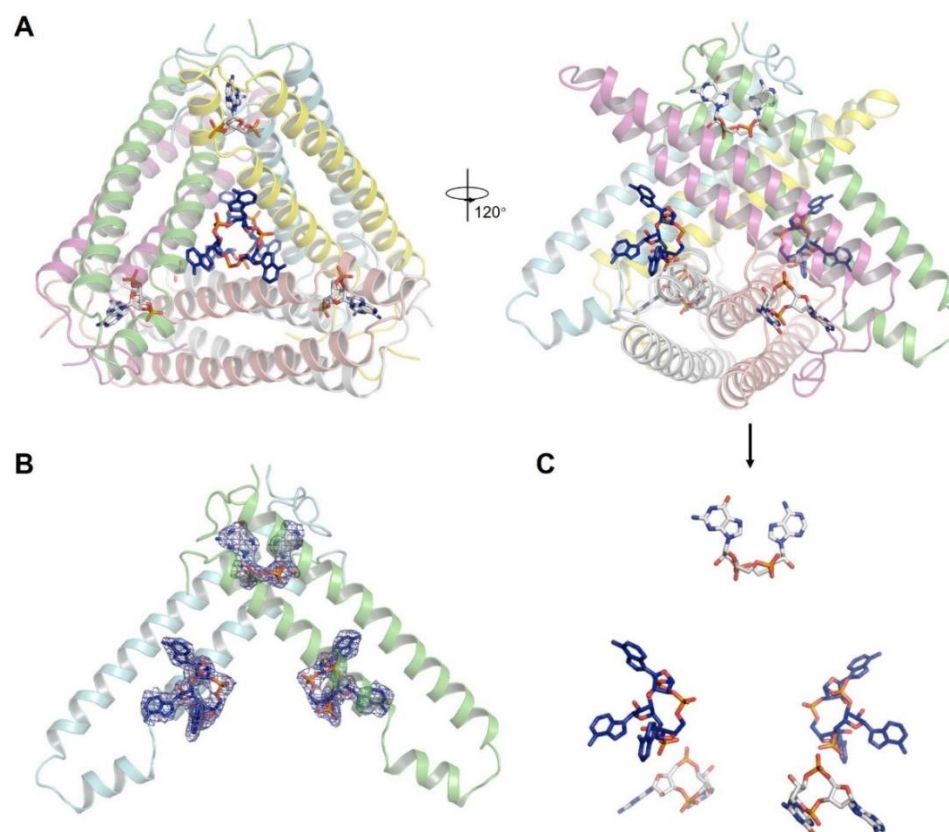
Figure 3. Acb2 binds to cyclic trinucleotides and dinucleotides simultaneously

(A) Overall structure of Acb2 complexed with cA_3 and 3',3'-cGAMP. cA_3 and 3',3'-cGAMP are shown as blue and light gray sticks. Two views are shown.

(B) 2Fo-Fc electron density of cA_3 and 3',3'-cGAMP within an Acb2 dimer contoured at 1 σ.

(C) Distribution of the small molecules within the Acb2 hexamer. The nucleotides are shown as they are in the right panel of (A).

## Acb2 binds to cA_3 with a novel fold

Dali search did not return entries of experimentally determined proteins with the same fold as Acb2, nor did Foldseek searches of computationally predicted proteins (van Kempen et al., 2023), suggesting that both the cyclic dinucleotide and trinucleotide-binding folds are novel. Several experimentally determined proteins have been reported to bind cyclic trinucleotides, including the CBASS effector proteins NucC (Lau et al., 2020) and Cap4 (Lowey et al., 2020) that directly bind cA_3, as well as the human CDN sensor RECON that directly binds cAAG (Whiteley et al., 2019). Compared to the cA_3 binding pocket in Acb2, those in NucC, Cap4, and RECON are significantly different. In NucC, one

220 cA$_3$ molecule is bound in a three-fold symmetric allosteric pocket at the "bottom" of the protein trimer,

221 mainly formed by an extended hairpin loop from each protomer. Additionally, each adenine base is

222 stabilized by hydrogen bonds and π stacking interactions in NucC (Figure S4A, PDB code: 6Q1H). In

223 Cap4, cA$_3$ is bound within its SAVED (SMODS-associated) domain, which is a fusion of two CARF

224 (CRISPR-associated Rossman fold) domains derived from Type III CRISPR-Cas system (Figure S4B,

225 PDB code: 6WAN). RECON adopts a TIM barrel fold with eight parallel β strands surrounded by eight

226 crossover α-helixes and cAAG is bound in a deep crevice at the top of the β barrel (Figure S4C, PDB

227 code: 6M7K). Moreover, the conformation of cA$_3$ within Acb2 is also different from those within NucC,

228 Cap4, and RECON complex structures (Figure S4D). Specifically, cA$_3$ in both NucC and Cap4 are

229 almost in an overall planar conformation, and two adenine bases of cAAG within RECON are nearly

230 in the same plane as the phosphodiester ring and the third guanine base is extended out. However, each

231 base of cA$_3$ forms a ~46.8 degree angle with the phosphate plane in Acb2. Together, the structure of

232 Acb2 complexed with cA$_3$ reveals a novel cyclic trinucleotide-binding fold.

233

234 Cyclic nucleotide binding spectra are different among Acb2 homologs

235 Compared to the highly conserved Y11 and K26 residues of Acb2 (essential for 3',3'-cGAMP binding)

236 found in the *Pseudomonas aeruginosa* phage PaMx33 protein, the R67 and T74 residues (essential for

237 cA$_3$ binding) are less conserved and vary in some Acb2 homologs (Figure 4A) (Huiting et al., 2023).

238 Therefore, we assessed the binding spectrum of other Acb2 homologs to determine whether the

239 homologs bind to the same spectrum of cyclic oligonucleotides. We chose Acb2 homologs from *P.*

240 *aeruginosa* phage JBD67 (44.4% a.a. identity), in which both R67 and T74 residues are conserved,

241 *Serratia* phage CHI14 (23.5% a.a. identity) and *Escherichia* phage T4 (24.2% a.a. identity), in which

242 only R67 (Serratia phage) or T74 (Escherichia phage) residue is conserved. ITC analyses showed that

243 JBD67-Acb2 directly binds to 3',3'-cGAMP with a K_D of ~99 nM and cA$_3$ with a K_D of ~3.5 nM

244 (Figure 4B and S5A-B), both of which are comparable to those of PaMx33-Acb2. Native gel assays

245 also suggest that JBD67-Acb2 binds to the same spectrum of cyclic nucleotides as PaMx33-Acb2

246 (Figure S6A). ITC analyses showed that T4-Acb2 directly binds to 3',3'-cGAMP with a K_D of ~84.4

247 nM, consistent with previous work (Jenson et al., 2023), but does not bind to cA$_3$ (Figure 4C and S5C-

248 D). Native gel assays also suggest that T4-Acb2 binds the same spectrum of cyclic dinucleotides as

249 PaMx33-Acb2, but not to the cyclic trinucleotides cA$_3$ and cAAG (Figure S6B). Next, we mutated

250   D61 of T4-Acb2 to Arginine to see whether it can endow T4-Acb2 with the binding activity of cA_3

251   because T4-Acb2 already has T68 residue in the place of T74 of PaMx33-Acb2 that is essential for

252   cA_3 binding. However, based on ITC assays, we observed that the D61R mutant of T4-Acb2 was still

253   unable to bind cA_3 (Figures 4C and S5E). Interestingly, structural alignment between T4-Acb2 (Jenson

254   et al., 2023) and PaMx33-Acb2 complexed with cA_3 showed that the helix lining the cA_3 binding

255   pocket of PaMx33-Acb2 has a kink at E64, which enlarges the pocket to accommodate the base groups

256   of cA_3 (Figure 4D). However, the corresponding helix of T4-Acb2 does not kink here, so the Y37, A57,

257   L60, D61 and T64 residues of T4-Acb2 may undergo steric clashing and prevent cA_3 binding (Figure

258   4D). More importantly, the relative angles among the three helices lining the binding pocket are also

259   different between PaMx33-Acb2 and T4-Acb2, resulting in a smaller binding pocket in T4-Acb2

260   (Figure 4E). Together, these observations may explain the inability of T4-Acb2 binding to cyclic

261   trinucleotides. Lastly, ITC analyses showed that CHI14-Acb2 directly binds to 3',3'-cGAMP with a

262   K_D of ~62.4 nM, but does not bind to cA_3 (Figure 4F). Of note, native gel assays showed almost no

263   shift of the CHI14-Acb2 protein upon adding any cyclic oligonucleotides, including 3',3'-cGAMP

264   (Figure S6C), suggesting that native gel assay is not suitable for studying the binding spectrum of

265   CHI14-Acb2. Therefore, we studied the binding of all the cyclic oligonucleotides to CHI14-Acb2

266   through ITC analyses, which showed that CHI14-Acb2 exhibits the same binding spectrum as T4-

267   Acb2 (Figures 4F-G and S7). In summary, Acb2 homologs bind to many cyclic trinucleotides and

268   dinucleotides used in cGAS-based immunity with certain homologs being more broad spectrum than

269   enzyme Acb1 (Figure 4H).
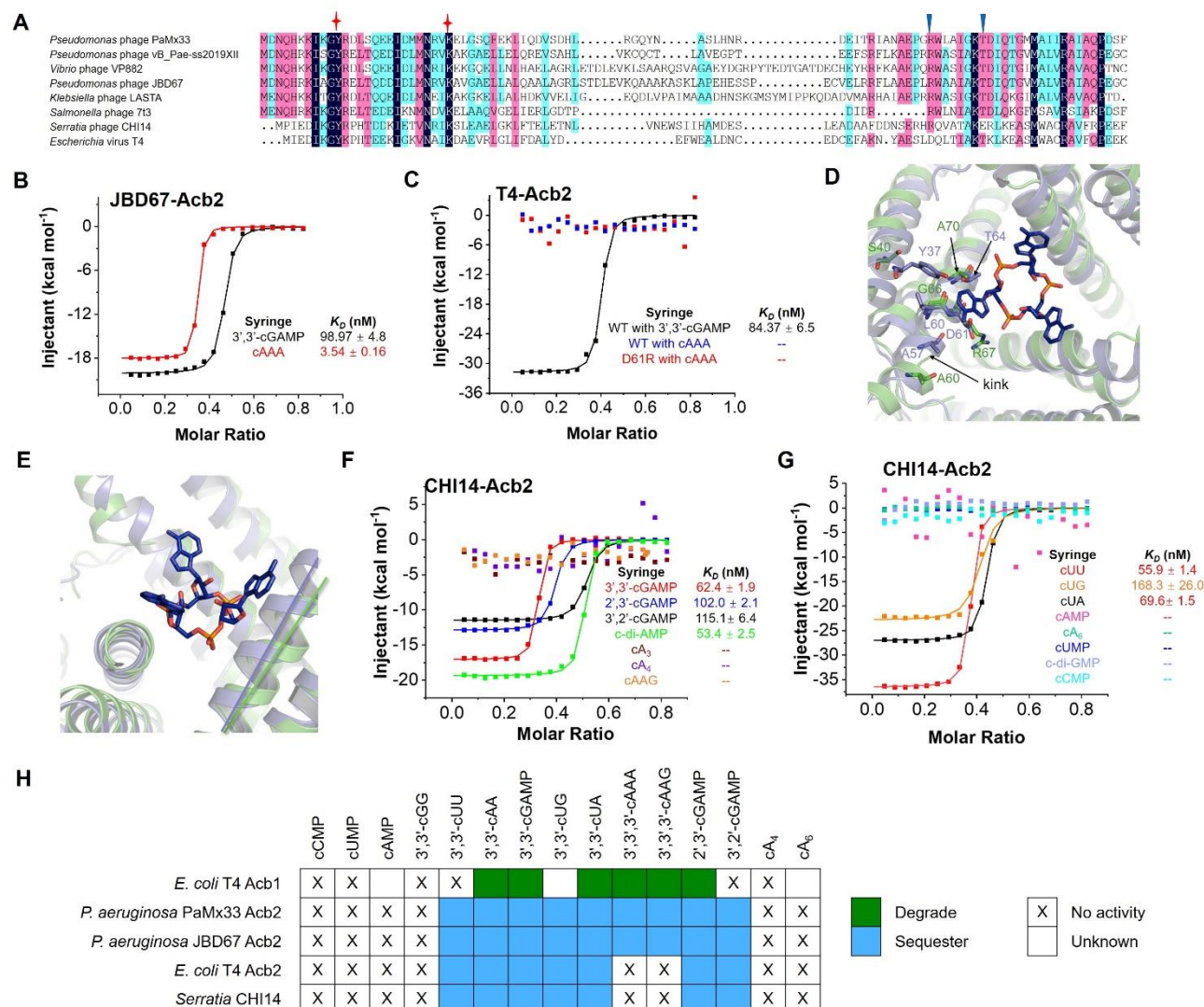
Figure 4. The binding spectra are different among Acb2 homologs

(A) Sequence alignment among Acb2 homologs. Residues with 100 % identity, over 75 % identity and over 50 % identity are shaded in dark blue, pink and cyan, respectively. Residues involved in binding of cyclic dinucleotides and trinucleotides are marked with stars and triangles, respectively.

(B) ITC assays to test binding of cyclic oligonucleotides to JBD67-Acb2. Representative binding curves and binding affinities are shown. The K_D values are mean ± s.d. (n=3). Raw data for these curves are shown in Figure S5.

(C) ITC assays to test binding of cyclic oligonucleotides to T4-Acb2. Representative binding curves and binding affinities are shown. The K_D values are mean ± s.d. (n=3). Raw data for these curves are shown in Figure S5.

(D) Structural alignment between PaMx33-Acb2 and T4-Acb2 at one monomer. Residues with potential steric clash with cA_3 in T4-Acb2 and the corresponding residues in PaMx33-Acb2 are shown

283 in sticks.

284 (E) The same alignment shown in (D), highlighting the different relative angels formed by the three

285 helices lining the binding pocket of cA_3.

286 (F-G) ITC assays to test binding of cyclic nucleotides to CHI14-Acb2. Representative binding curves

287 and binding affinities are shown. The K_D values are mean ± s.d. (n=3). Raw data for these curves are

288 shown in Figure S6.

289 (H) Summary of the binding results of Acb2 homologs and Acb1 (Hobbs et al., 2022).

290

291 Acb2 antagonizes Type III-C CBASS immunity

292 Since Acb2 displays high affinity binding to cyclic trinucleotides, we tested whether phage-encoded

293 Acb2 can inhibit Type III-C CBASS immunity that uses a cA_3 signaling molecule to activate

294 endonuclease (NucC) effector protein. NucC is a cyclic nucleotide-activated effector in both CBASS

295 and Type III CRISPR-Cas systems, where it non-specifically degrades DNA and prematurely kill the

296 host cell before phage can effectively replicate (Lau et al., 2020; Mayo-Muñoz et al., 2022; Ye et al.,

297 2020). First, we set up an *in vitro* NucC activity assay using purified NucC from the *P. aerginosa*

298 strain ATCC 27853. While cA_3 activates the DNA cleavage activity of NucC, adding WT Acb2 into

299 this system significantly decreased NucC activity (Figure 5A). Moreover, following proteolysis of WT

300 Acb2, the released cA_3 molecule again activated the NucC activity (Figure 5A; last two lanes). The

301 R67A and T74A Acb2 mutant proteins, which lost or exhibited decreased cA_3 binding, displayed

302 minimal inhibition of NucC activity. However, the Y11A and K26A Acb2 mutants, whose cyclic

303 dinucleotide binding pockets are disrupted, inhibited NucC activity similarly to WT Acb2 (Figure 5A).

304 These results demonstrate that Acb2 antagonizes Type III-C CBASS immunity *in vitro* through

305 sequestering the cA_3 molecule.

306

307 To determine whether phage-encoded Acb2 can inhibit this same cA_3-based CBASS system *in vivo,*

308 we performed phage infection assays with the *P. aeruginosa* ATCC 27853 strain harboring the Type

309 III-C CBASS operon (Figure 5B). However, phages naturally expressing *acb2* were unable to

310 replicate on the native *P. aeruginosa* strain, which is likely due to the presence of other anti-phage

311 immune systems (Huiting et al. 2023), prophages, or receptor incompatibility. Next, we established a

312 heterologous host expressing the *P. aeruginosa* ATCC 27853 (Pa278) Type III-C CBASS operon in a

313 phage sensitive strain that naturally lacks CBASS (PAO1). We also used a *P. aeruginosa* strain with a

314 chromosomally integrated BWHPSA011 (Pa011) Type II-A CBASS operon (3',3'-cGAMP-

315 producing), which Acb2 has been shown to antagonize (Huiting et al. 2023). In the presence of Pa278

316 Type III-C CBASS, WT JBD67 phage encoding Acb2 was unaffected, but the *acb2* mutant phage

317 (JBD67Δ*acb2*) was reduced 4 orders of magnitude (Figures 5C-D), demonstrating potent Acb2 activity

318 *in vivo* against a trinucleotide system.   In the presence of the Pa011 Type II-A CBASS system, JBD67

319 WT phage titer was reduced by ~1 order of magnitude, consistent with Acb2 being partially

320 overwhelmed, as shown previously (Huiting et al. 2023). This finding supports a hypothesis from

321 Jenson et al., 2023 that proposes ubiquitin-like conjugation of the Type II-A CBASS CD-NTase

322 enhances cGAMP production to overwhelm the CDN sponge (Jenson et al., 2023). By contrast, the

323 titer of the *acb2* mutant phage was reduced 5 orders of magnitude (Figures 5C-D), which confirms the

324 potent, yet incomplete, inhibition of Type II-A CBASS. Co-expression of Pa278 Type III-C CBASS

325 (cA$_3$ producing) and Pa011 Type II-A CBASS (3',3'-cGAMP producing) targets the WT JBD67 phage

326 to the same degree as Pa011 Type II-A CBASS alone (Figures 5C-D), demonstrating the versatility of

327 Acb2 when simultaneously faced with two distinct CBASS systems *in vivo*.

328
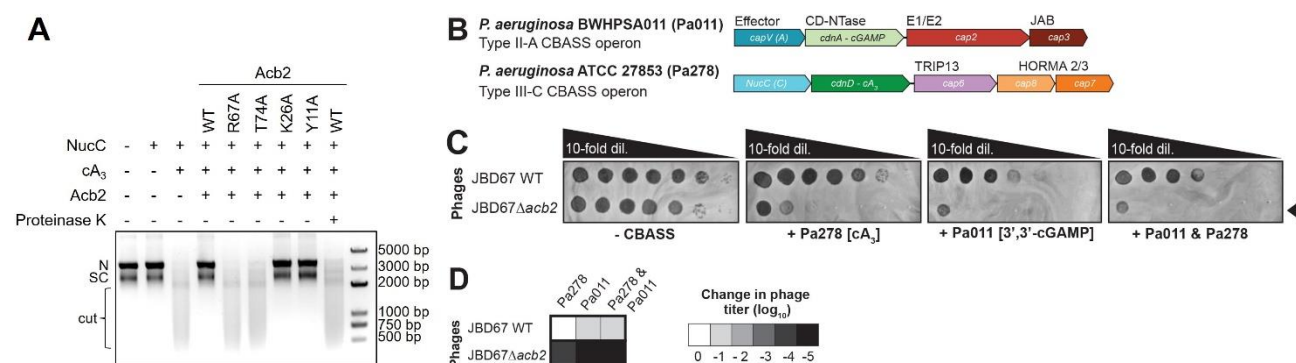
330 **Figure 5. Acb2 antagonizes tri- and di-nucleotide based CBASS immunity**

331 (A) Effect of Acb2 or its mutants on cA$_3$-activated NucC effector protein function. After treatment with

332 proteinase K, the released cA$_3$ also showed the ability to activate the nuclease activity of NucC. The

333 concentration of NucC, cA$_3$, Acb2 and proteinase K is 10 nM, 5 nM, 50 nM and 1 μM, respectively.

334 N denotes nicked plasmid, SC denotes closed-circular supercoiled plasmid, and cut denotes fully

335 digested DNA.

336 (B) *Pseudomonas aeruginosa* BWHPSA011 (Pa011) Type II-A CBASS and ATCC 27853 (Pa278)

337   Type III-C CBASS operons.

338   (C) Plaque assays with JBD67 WT and Δ*acb2* phages spotted in 10-fold serial dilutions on a lawn of

339   PAO1 strain harboring an empty vector (E.V.) plasmid (-CBASS), PAO1 harboring a plasmid with the

340   Pa278 CBASS operon (+ Pa278), PAO1 with a chromosomally integrated Pa011 CBASS operon (+

341   Pa011), and the aforementioned strain harboring a plasmid with the Pa278 CBASS operon (+ Pa011

342   & Pa278). Basal expression of both operons was sufficient to induce phage targeting (i.e. induction

343   was not necessary).

344   (D) Heat map representing the order of magnitude change in phage titer, where phage titer is quantified

345   by comparing the number of spots (with plaques, or clearings if plaques were not visible) on the

346   CBASS-expressing strains divided by the E.V.-expressing strain (n=3).

347

348   **Discussion**

349   Following phage infection, CBASS immunity functions via the activation of a cGAS-like enzyme to

350   catalyze the synthesis of a cyclic oligonucleotide signaling molecule. To date, two phage proteins have

351   been discovered to antagonize the CBASS immunity: Acb1 and Acb2. Acb1 uses an inhibitory

352   mechanism common to the eukaryotic cGAS-STING signaling system (Eaglesham and Kranzusch,

353   2020), that is, enzymatically cleaving and depleting an array of cyclic dinucleotides and trinucleotides

354   (Hobbs et al., 2022). In contrast, we, alongside another independent group, reported that Acb2 acts as

355   a "sponge" and sequesters 3',3'-cGAMP (Huiting et al., 2023; Jenson et al., 2023) as well as a variety

356   of other CBASS cyclic dinucleotide signaling molecules (Huiting et al., 2023). A sponging mechanism

357   was also reported for inhibitors of the anti-phage system Thoeris, including Tad1 (Leavitt et al., 2022)

358   and Tad2 (Yirmiya et al., 2023). Here, we extend the dinucleotide binding spectrum to include 3',2'-

359   cGAMP, a signaling molecule not cleaved by Acb1, but recently implicated in both CBASS and cGAS

360   like signaling in eukaryotes (Cai et al., 2023; Fatma et al., 2021; Slavik et al., 2021). The ability of

361   Acb2 to function in human cells reinforces the flexibility of the "sponging" mechanism (i.e. no need

362   to bind to CBASS proteins or host machinery), and the remarkable trans-kingdom conservation of this

363   cyclic-oligonucleotide-based immune system. These data also open up the possibility that pathogenic

364   bacteria encoding Acb1, Acb2, or other undiscovered cGAMP interactors (i.e. on prophages) could use

365   them to dampen the human immune response during intracellular infection. Indeed, cross-kingdom

366   signaling has been previously reported with bacterial c-di-GMP   (Burdette et al., 2011) and c-di-AMP

367 produced by *Listeria monocytogenes* (Woodward et al., 2010), which both serve as ligands for human

368 STING.   Taken together, these observations suggests that the interface between the bacterial signals,

369 cyclic oligonucleotide inhibitors, and cGAS-STING immunity has yet to be fully explored.

370

371 Acb2 binds to and sequesters cyclic trinucleotides with a magnitude higher binding affinity than to

372 dinucleotides. Based on this finding, we further observed that Acb2 binds to a wider spectrum of cyclic

373 oligonucleotides compared to the enzyme Acb1 including 3',3'-cUU, 3',3'-cUG, and 3',2'-cGAMP

374 (Figure 4H). Moreover, Acb2 uses distinct, independent binding pockets to sequester cyclic

375 dinucleotides and trinucleotides whereas Acb1 uses the same active site to degrade cyclic

376 oligonucleotides. In some cases, however, we observed that Acb2 homologs cannot bind to cyclic

377 trinucleotides. Although it is unclear if there is a cost to the trinucleotide binding site that would lead

378 to its loss, in the case of phage T4, its genome encodes both Acb1 and Acb2 and therefore suggests

379 that this phage is broadly evasive of most CBASS systems. To our knowledge, Acb2 represents the

380 first protein that can simultaneously bind two types of cyclic oligonucleotides with different binding

381 pockets. Altogether, our work highlights Acb2 as an effective and potent inhibitor of nearly all CBASS

382 types, with great potential to fortify phage therapeutics by enabling evasion of most cGAS-based anti-

383 phage systems in bacteria.

384

397   the Vallee Foundation, and the Searle Scholarship.

398

399   **Author contributions:**

400   Y.F. and J.B.-D. conceived and supervised the project and designed experiments.   Xueli Cao, D. L.,

401   Y. W. and L. G. purified the proteins, grew and optimized the crystals, collected the diffraction data,

402   and performed *in vitro* activity analysis and binding assays. Y.X. solved the crystal structures. E.H.

403   performed all *in vivo* phage experiments. J.R. performed the HPLC analysis. Xujun Cao performed *in*

404   *vivo* human cell experiments under supervision of L.L.. Y.F. wrote the original manuscript. J.B.-D.,

405   Y.F., and E.H. revised the manuscript.

406

407   **Declaration of interests:** J.B.-D. is a scientific advisory board member of SNIPR Biome and Excision

408   Biotherapeutics, a consultant to LeapFrog Bio, and a scientific advisory board member and co-founder

409   of Acrigen Biosciences. The Bondy-Denomy lab received research support from Felix Biotechnology.

410   UCSF has filed a patent application related to this work with J.B.-D. and E.H. listed as inventors.

411

412

413

414

415

416

417

418

419

420

421

422

423

424

425

Table 1. Data collection and refinement statistics

Data set	Acb2-2',3'-cGAMP	Acb2-3',2'-cGAMP	Acb2-cA$_3$	Acb2-cAAG	Acb2-3',3'-cGAMP-cA$_3$
PDB code	8J8O	8IXZ	8IY0	8IY1	8IY2
Data collection					
Space group	P321	P321	P321	P321	P321
Cell dimensions					
a, b, c (Å)	106.0 106.0 101.6	104.0 104.0 101.1	103.9 103.9 101.9	103.6 103.6 101.4	103.4 103.4 101.5
α, β, γ (°)	90.0 90.0 120.0	90.0 90.0 120.0	90.0 90.0 120.0	90.0 90.0 120.0	90.0 90.0 120.0
Resolution (Å)	50-2.24 (2.28-2.24)	50-2.32 (2.36-2.32)	50-2.26 (2.30-2.26)	50-2.10 (2.14-2.10)	50-2.76 (2.81-2.76)
Unique reflections	31815 (1484)	27614 (1352)	29547 (1474)	36272 (1648)	16565 (824)
Completeness (%)	99.5 (94.3)	100.0 (100.0)	98.7 (99.1)	98.1 (92.8)	99.7 (100.0)
Rmeas (%)	10.6 (96.7)	8.4 (60.8)	12.3 (103.7)	9.9 (87.9)	13.3 (101.2)
Redundancy	4.8 (3.9)	17.6 (13.1)	4.8 (4.8)	17.6 (13.6)	9.8 (8.9)
$I/\sigma(I)$	18.2 (1.4)	50.0 (4.8)	18.3 (2.2)	47.9 (4.1)	20.8 (2.5)
Statistics for Refinement					
Rwork (%)	23.8 (32.4)	23.0 (27.3)	21.5 (25.2)	22.1 (24.6)	24.0 (34.8)
Rfree (%)	27.3 (34.6)	27.4 (32.6)	25.8 (35.0)	24.9 (28.8)	28.9 (40.1)
No. atoms	4915	4741	5019	5072	5051
Protein	4416	4396	4440	4440	4396
Ligand/ion	270	270	396	402	628
Solvent	229	75	183	230	27
B factors	51.90	55.65	48.17	45.56	57.43
Protein	52.14	56.07	49.77	47.10	58.87

Ligand/ion	50.60	51.32	33.26	31.55	47.68
Solvent	47.16	47.03	41.65	40.42	49.83
R.m.s.d.					
Bond angles (°)	1.49	2.49	2.37	2.90	2.42
Bond length (Å)	0.013	0.016	0.014	0.029	0.016
Ramachandran plot(%)					
Favored region	99.07	96.26	97.59	96.67	97.01
Allowed region	0.93	3.74	2.41	3.33	2.99
Outliers	0.00	0.00	0.00	0.00	0.00

426

427

428

429

430 **STAR Methods:**

431 **Key Resources Table**

Resource or Reagent	Description	Source and/or Reference	ID
Bacterial and virus strains			
P. aeruginosa BWHPSA011 (Pa011) WT		Deborah Hung Lab	NCBI: NZ_AXQR01000000.1
P. aeruginosa ATCC 27853 (Pa278) WT		ATCC	NCBI: CP015117.1
P. aeruginosa PAO1 WT		Joe Bondy-Denomy Lab	NCBI: NC_002516.2

PAO1 + chromosomally integrated Pa011 CBASS operon		Joe Bondy-Denomy Lab (Huiting et al., 2023)	N/A
JBD67		Alan Davidson Lab (Cady et al., 2012)	NCBI: NC_042135.1
JBD67Δ*acb2* (Removal of 23005-23232 bp *orf24* (*acb2*))		Joe Bondy-Denomy Lab (Huiting et al., 2023)	N/A
Mammalian cell lines			
HEK293T Dual-Null		Invivogen	Cat#: 293d-null
Recombinant DNA			
pET28a-His$_6$-SUMO-PaMx33-Acb2		This study	N/A
pET28a-His$_6$-SUMO-PaMx33-Acb2 Y11A		This study	N/A
pET28a-His$_6$-SUMO-PaMx33-Acb2 K26A		This study	N/A
pET28a-His$_6$-SUMO-PaMx33-Acb2 T74A		This study	N/A
pET28a-His$_6$-SUMO-PaMx33-Acb2 R67A		This study	N/A
pET28a-His$_6$-SUMO-JBD67-Acb2		This study	N/A

pET28a-His$_6$-CHI14-Acb2		This study	N/A
pET28a-His$_6$-CHI14-Acb2 E76T		This study	N/A
pET28a-His$_6$-CHI14-Acb2 E76T/R67P		This study	N/A
pET28a-His$_6$-SUMO-T4-Acb2		This study	N/A
pET28a-His$_6$-SUMO-T4-Acb2 D61R		This study	N/A
pHERD30T (p30T)		(Qiu et al., 2008)	N/A
p30T-Pa011 Type II-A CBASS (1250416-1255003; Contig 12)		This study	N/A
P30T-Pa27853 Type III-C CBASS (6283357-6286926)		This study	N/A
pcDNA3		Lingyin Li Lab	N/A
pcDNA3-hSTING-232R		Lingyin Li Lab	N/A
pcDNA3-AcbIIA2 WT		This paper	N/A
pcDNA3-AcbIIA2 Y11A		This paper	N/A
pcDNA3-AcbIIA2 K26A		This paper	N/A
Chemicals, peptides, and recombinant proteins			

Phusion High-Fidelity DNA polymerase		NEB	Cat #M0530S
dNTPs		NEB	Cat #N0447S
Phusion GC Buffer		NEB	Cat #B0519
Gibson Assembly HiFi DNA Master Mix		NEB	Cat #E2621
SacI		NEB	Cat #R3156S
PstI		NEB	Cat #R3140S
HEPES sodium salt		Sigma-Aldrich	CAS: 7365-45-9 Cat #: V900477-500G
Tris base		Sigma-Aldrich	CAS: 77-86-1 Cat #: RDD008-2.5KG
Sodium dihydrogen phosphate dihydrate		Sigma-Aldrich	CAS: 13472-35-0 Cat #: 1063420250
Disodium hydrogen phosphate dodecahydrate		Sigma-Aldrich	CAS: 10039-32-4 Cat #: 1065790500
Bis-Tris propane		Sigma-Aldrich	CAS: 64431-96-5 Cat #: B6755-25G
Sodium bromide		Sigma-Aldrich	CAS: 7647-15-6 Cat #: 310506-100G
PEG 3350		Biorigin	CAS: 25322-68-3 Cat #: BN33640
Glycerol		Sigma-Aldrich	CAS: 56-81-5

			Ca t#: V900122-500ML
Imidazole		Sigma-Aldrich	CAS: 288-32-4 Cat #: V900153-500G
2× Phanta Max Master Mix	Used for protein expression experiments	Vazyme	Cat #: P515-03
2× Rapid Taq Master Mix	Used for protein expression experiments	Vazyme	Cat #: P222-AA
KOD-Plus-Neo		TOYOBO	Cat #: KOD-401
DpnI		NEB	Cat #: R0176S
Proteinase K		NEB	Cat #: P8107S
High Affinity Ni-NTA Resin		GenScript	Cat #: L00250-100
a-tubulin (DM1A), Mouse mAb		Sigma-Aldrich	Cat# T6199; RRID:AB_477583
STING (D2P2F) Rabbit mAb		Cell Signaling Technologies	Cat# 13647; RRID: AB_2732796
Acb2 custom polyclonal antibody		GenScript	N/A
Goat Anti-Mouse IgG Antibody, IRDye® 680RD Conjugated		Li-COR Biosciences	Cat# 926-68070; RRID: AB_10956588

IRDye 800CW Goat anti-Rabbit IgG (H+L)		Li-COR Biosciences	Cat# 925-32211; RRID: AB_2651167
PaMx33-Acb2 WT recombinant protein		This study	N/A
PaMx33-Acb2^{Y11A} recombinant protein		This study	N/A
PaMx33-Acb2^{R67A} recombinant protein		This study	N/A
PaMx33-Acb2^{T74A} recombinant protein		This study	N/A
PaMx33-Acb2^{K26A} recombinant protein		This study	N/A
CHI14-Acb2 WT recombinant protein		This study	N/A
JBD67-Acb2 WT recombinant protein		This study	N/A
T4-Acb2 WT recombinant protein		This study	N/A
T4-Acb2 ^{D61R} recombinant protein		This study	N/A
Critical Commercial Assays			
Plasmid Miniprep Kit	Used for protein expression experiments	Vazyme	Cat #: DC201-01

Gel DNA Extraction Mini Kit	Used for protein expression experiments	Vazyme	Cat #: DC301-01
QUANTI-Luc		Invivogen	Cat #: rep-qlc2
Deposited Data			
Structure of		This study	PDB:
Oligonucleotides			
3',3'-cGAMP		Sigma-Aldrich	CAS: 849214-04-6 Cat #: SML1232-.5UMO
2',3'-cGAMP		Sigma-Aldrich	CAS:1441190-66-4 Cat #SML1229-.5UMO
c-di-AMP		Sigma-Aldrich	CAS: 54447-84-6 Cat #SML1231-1UMO
c-di-GMP		Sigma-Aldrich	CAS: 61093-23-0 Cat #SML1228-1UMO
3',3'-c-UMP-GMP		Biolog Life Science Institute	CAS: 232933-52-7 Cat #C371
3',3'-c-di-UMP		Biolog Life Science Institute	CAS: 73120-97-5 Cat #C256
3',3'-c-UMP-AMP		Biolog Life Science Institute	CAS: 83799-66-0 Cat #C357
3',2'-cGAMP		Biolog Life Science Institute	CAS: 1615704-64-7 Cat #C238

3',3',3'-cAAG		Biolog Life Science Institute	CAS: 2365165-54-2 Cat #C361
3',3',3'-cAAA (cA$_3$)		Biolog Life Science Institute	CAS: 54447-85-7 Cat #C362
cA$_4$		Biolog Life Science Institute	CAS: 118004-81-2 Cat #C335
cA$_6$		Biolog Life Science Institute	CAS: 232933-63-0 Cat #C332
cAMP		MedChemExprss	CAS: 60-92-4 Cat #HY-B1511S
cUMP		Sigma-Aldrich	CAS: 56632-58-7 Cat #SML3286-50UMOL
Y11A_F 5'– gcacaagaaaatcaagggcgccag agatctgtctcagga–3'	Quikchange Primer	This study	N/A
Y11A_R 5'– ctcctgagacagatctctggcgccct tgattttcttgtgc–3'	Quikchange Primer	This study	N/A
K26A_F 5'– gacatgatgaacagagtggcggaa ctgggcagccagtt–3'	Quikchange Primer	This study	N/A
K26A_R 5'– aactggctgcccagttccgccactct gttcatcatgtc–3'	Quikchange Primer	This study	N/A
Software and algorithms			

National Center for Biotechnology Information (NCBI) database		(Sayers et al., 2022)	https://blast.ncbi.nlm.nih.gov/
NCBI Multiple Sequence Alignment Viewer (MSA)		MSA Software	https://www.ncbi.nlm.nih.gov/tools/msaviewer/
NCBI Constraint-based Multiple Alignment Tool (COBALT)		(Papadopoulos and Agarwala, 2007)	https://www.ncbi.nlm.nih.gov/tools/cobalt/re_cobalt.cgi
HKL2000		(Otwinowski and Minor, 1997)	http://www.hkl-xray.com/
PHENIX		(Adams et al., 2002)	http://www.phenix-online.org
COOT		(Emsley et al., 2010)	http://www2.mrc-lmb.cam.ac.uk/personal/pemsley/coot
PyMOL		The PyMOL Molecular Graphics System, Version 2.5.2., Schrodinger, LLC	https://pymol.org/2/
DALI		(Holm, 2022)	http://ekhidna2.biocenter.helsinki.fi/dali/
Foldseek		(van Kempen et al., 2023)	https://search.foldseek.com/search
OriginPro 8		OriginPro Software	N/A

GraphPad Prism 9		GraphPad Software	https://www.graphpad.com/
Other			
Amicon Ultra-0.5 centrifugal filter unit		Merck	Cat #: UFC500396
Amicon concentrators (3 K)		Millipore	Cat #: UFC800308
Amicon concentrators (10 K)		Millipore	Cat #: UFC901096
Amicon concentrators (30 K)		Millipore	Cat #: UFC903024
HisTrap FF (5 mL)		GE Healthcare	Cat #: 17-5255-01
HiTrap Heparin HP (5 mL)		GE Healthcare	Cat #: 17-0407-03
HiTrap Q Sepharose FF (5 mL)		GE Healthcare	Cat #: 17-5156-01
Superdex 200 increase 10/300 GL		GE Healthcare	Cat #: 17517501

432

433

434 **RESOURCE AVAILABILITY**

435 **Materials Availability**

436 All unique/stable reagents generated in this study are available from the Lead Contact with a completed

437 Materials Transfer Agreement.

438

439 **Data and Code Availability**

440 The accession numbers for the coordinate and structure factors reported in this paper are PDB: 8IXZ

441 (Acb2-3',2'-cGAMP), 8J8O (Acb2-2',3'-cGAMP), 8IY0 (Acb2-cA$_3$), 8IY1 (Acb2-cAAG) and 8IY2

442 (Acb2-3',3'-cGAMP-cA$_3$). This paper does not report original code. Any additional information

443 required to reanalyze the data reported in this paper is available from the lead contact upon request.

444

445 **EXPERIMENTAL MODEL AND SUBJECT DETAILS**

446 **Bacterial strains and phages**

447 The bacterial strains and phages used in this study are listed in the Key Resources Table. The *P.*

448 *aeruginosa* strains (BWHPSA011, ATCC 27853, PAO1) and *E. coli* strains (DH5α) were grown in

449 Lysogeny broth (LB) medium at 37°C both with aeration at 225 r.p.m. Plating was performed on LB

450 solid agar with 10 mM MgSO$_4$ when performing phage infections, and when indicated, gentamicin (50

451 µg ml^{-1} for *P. aeruginosa* and 15 µg ml^{-1} for *E. coli*) was used to maintain the pHERD30T plasmid.

452 Gene expression was induced by the addition of L-arabinose (0.1%) unless stated otherwise. The *E.*

453 *coli* BL21 (DE3) strain was used for recombinant protein overexpression and grown in Lysogeny broth

454 (LB) medium. The cells were grown at 37°C until OD$_{600nm}$ reached 0.8 and then induced at 18°C for

455 12 h.

456

457 **METHOD DETAILS**

458 **Protein expression and purification**

459 The PaMx33-Acb2, JBD67-Acb2, T4-Acb2, and CHI14-Acb2 genes were synthesized by GenScript.

460 The full-length Acb2 gene was amplified by PCR and cloned into a modified pET28a vector in which

461 the expressed Acb2 protein contains a His$_6$-SUMO tag or His$_6$ tag. The Acb2 mutants were generated

462 by two-step PCR and were subcloned, overexpressed and purified in the same way as wild-type protein.

463 The proteins were expressed in *E. coli* strain BL21 (DE3) and induced by 0.2 mM isopropyl-β-D-

464 thiogalactopyranoside (IPTG) when the cell density reached an OD$_{600nm}$ of 0.8. After growth at 18°C

465 for 12 h, the cells were harvested, re-suspended in lysis buffer (50 mM Tris–HCl pH 8.0, 300 mM

466 NaCl, 10 mM imidazole and 1 mM PMSF) and lysed by sonication. The cell lysate was centrifuged at

467 20,000 g for 50 min at 4°C to remove cell debris. The supernatant was applied onto a self-packaged

468 Ni-affinity column (2 mL Ni-NTA, Genscript) and contaminant proteins were removed with wash

469 buffer (50 mM Tris pH 8.0, 300 mM NaCl, 30 mM imidazole). The fusion protein of Acb2 with His$_6$-

470   SUMO tag was then digested with Ulp1 at 18°C for 2 h, and then the Acb2 protein was eluted with

471   wash buffer. The eluant of Acb2 was concentrated and further purified using a Superdex-200 increase

472   10/300 GL (GE Healthcare) column equilibrated with a buffer containing 10 mM Tris-HCl pH 8.0, 500

473   mM NaCl and 5 mM DTT. The purified protein was analyzed by SDS-PAGE. The fractions containing

474   the target protein were pooled and concentrated.

475

476   The His_6-Acb2 proteins bound to Ni-NTA beads were washed with wash buffer (50 mM Tris pH 8.0,

477   300 mM NaCl, 30 mM imidazole) and then eluted with the 50 mM Tris pH 8.0, 300 mM NaCl, 300

478   mM imidazole. The eluant of His_6-Acb2 was concentrated, then further purified and analyzed as

479   described above.

480

481   **Crystallization, data collection and structural determination**

482   The crystals of Acb2 were grown with reservoir solution containing 0.2 M Sodium bromide, 0.1 M

483   Bis-Tris propane pH 6.5, 10% Ethylene glycol and 20% v/v PEG 3350 at 18°C. Prior to

484   crystallization, cA_3, cAAG, cA_3+3',3'-cGAMP or 3',2'-cGAMP were mixed with the protein at a

485   molar ratio of 2:1, respectively, and the concentration of Acb2 was 24 mg/mL. The crystals appeared

486   overnight and grew to full size in about two to three days. The crystals were cryoprotected in the

487   reservoir solution containing 20% glycerol before its transferring to liquid nitrogen.

488

489   All the data were collected at SSRF beamlines BL02U1 and BL19U1, integrated and scaled using the

490   HKL2000 package (Otwinowski and Minor, 1997). The initial model of Acb2 was used from PDB:

491   8H2X. The structures of Acb2 and its complex with cyclic oligonucleotides were solved through

492   molecular replacement and refined manually using COOT (Emsley et al., 2010). The structure was

493   further refined with PHENIX (Adams et al., 2002) using non-crystallographic symmetry and

494   stereochemistry information as restraints. The final structure was obtained through several rounds of

495   refinement. Data collection and structure refinement statistics are summarized in Table 1.

496

497   **Isothermal titration calorimetry binding assay**

498   The dissociation constants of binding reactions of Acb2 or Acb2 mutants with the cA_3/ cAAG/ 3',2'-

499   cGAMP/ 3',3'-cGAMP/ 2',3'-cGAMP/ c-di-AMP/ c-di-GMP/ 3',3'-cUU/ 3',3'-cUA/ 3',3'-cUG/

500 cUMP/ cCMP/ cAMP/ cA_6/ cA_4 were determined by isothermal titration calorimetry (ITC) using a

501 MicroCal ITC200 calorimeter. Both proteins and cyclic-oligonucleotides were desalted into the

502 working buffer containing 20 mM HEPES pH 7.5 and 200 mM NaCl. The titration was carried out

503 with 19 successive injections of 2 μL cA_3/cAAG/cA_6/cA_4 at the 0.04 mM concentration, spaced 120 s

504 apart, into the sample cell containing the Acb2 or Acb2 mutants with a concentration of 0.01 mM by

505 700 rpm at 25°C. Correspondingly, the 3',2'-cGAMP/3',3'-cGAMP/2',3'-cGAMP/c-di-AMP/c-di-

506 GMP/3',3'-cUU/ 3',3'-cUA/3',3'-cUG/cUMP/cAMP at the 0.4 mM concentration was titrated   into

507 0.1 mM Acb2 or Acb2 mutants at the same experimental conditions. The Origin software was used for

508 baseline correction, integration, and curve fitting to a single site binding model.

509

510 **Native-PAGE assay**

511 Acb2 or Acb2 mutants was pre-incubated with cyclic-dinucleotides for 10 min at 18°C, where Acb2

512 or Acb2 mutants was 14.3 μM and the concentrations of cyclic-dinucleotides ranged from 1.8 to 7.2

513 μM (1.8, 3.6, 7.2 μM). Products of the reaction were analyzed using 5% native polyacrylamide gels

514 and visualized by Coomassie blue staining.

515

516 **High-performance liquid chromatography (HPLC)**

517 40 μM Acb2 or Acb2 mutants was pre-incubated with 4 μM cA_3 for 10 min at 18°C. Proteinase K was

518 subsequently added to the reaction system at a final concentration of 0.5 μM and the reaction was

519 performed at 58°C for 1 h. Reaction products were transferred to Amicon Ultra-15 Centrifugal Filter

520 Unit 3 kDa and centrifuged at 4°C, 4,000 g. The products obtained by filtration were further filtered

521 with a 0.22 μm filter and subsequently used for HPLC experiments. The HPLC analysis was performed

522 on an Agilent 1200 system with a ZORBAX Bonus-RP column (4.6 × 150 mm). A mixture of

523 acetonitrile (2%) and 0.1% trifluoroacetic acid solution in water (98%) were used as mobile phase with

524 0.8 mL/min. The compounds were detected at 254 nm.

525

526 ***In vitro* NucC activity assay**

527 For nuclease activity assay, a pUC19 plasmid was used as substrate. Pa-NucC (10 nM) and cA_3

528 molecules (5 nM) were mixed with 0.5 μg DNA in a buffer containing 25 mM Tris-HCl pH 8.0, 10

529 mM NaCl, 10 mM $MgCl_2$, and 2 mM DTT (20 μL reaction volume), incubated 10 min at 37°C, then

530   separated on a 1% agarose gel. Gels were stained with Goldview and imaged by UV illumination.

531

532   To determine the function of Acb2, 50 nM Acb2 or its mutants were pre-incubated with the system at

533   18°C for 15 min, and the subsequent reaction and detection method was as described above. To

534   examine whether the released molecule from Acb2 is able to activate NucC, 5 nM cA_3 was incubated

535   with 50 nM Acb2 for 15 min at 18°C. Proteinase K was subsequently added to the reaction system at

536   a final concentration of 1 μM and the reaction was performed at 58°C for 1 h, then the proteinase K-

537   treated samples were heated with 100°C for 10 min to extinguish proteinase K and the subsequent

538   detection method was as described above.

539

540   **Episomal gene expression**

541   The shuttle vector that replicates in *P. aeruginosa* and *E. coli*, pHERD30T (Qiu et al., 2008) was used

542   for cloning and episomal expression of *P. aeruginosa* BWHPSA011 Type II-A or ATCC 27853 Type

543   III-C CBASS operons into the PAO1 WT strain. This vector has an arabinose-inducible promoter and

544   a selectable gentamicin marker. Vector was digested with SacI and PstI restriction enzymes and then

545   purified. Inserts were amplified by PCR using bacterial overnight culture or phage lysate as the DNA

546   template, and joined into the pHERD30T vector at the SacI-PstI restriction enzyme cut sites by Hi-Fi

547   DNA Gibson Assembly (NEB) following the manufacturer's protocol. The resulting plasmids were

548   transformed into *E. coli* DH5α. All plasmid constructs were verified by sequencing using primers that

549   annealed to sites outside the multiple cloning site. *P. aeruginosa* cells were electroporated with the

550   pHERD30T constructs and selected on gentamicin.

551

552   **Plaque assays**

553   Plaque assays were conducted at 37°C with solid LB agar plates. 150 μL of overnight bacterial culture

554   was mixed with top agar and plated. Phage lysates were diluted 10-fold then 2 μL spots were applied

555   to the top agar after it had been poured and solidified.

556

557   **Interferon reporter assay in human cell line**

558   The PaMx33-Acb2 gene was codon-optimized for human expression and synthesized by GenScript

559   with overhangs that enabled insertion into the XhoI–BamHI sites of pcDNA3 via Gibson assembly.

560   The wild-type plasmid was modified by site-directed mutagenesis using the QuikChange protocol with

561   the indicated primers, and Dpn1-digested to obtain all point mutants. All recombinant plasmids were

562   transformed into XL1-Blue competent cells (Agilent) and sequenced for verification.

563

564   293T-Dual Null cells were cultured in DMEM (Gibco) supplemented with 10% FBS (Atlanta Biologics)

565   (v/v) and 100 U/mL penicillin-streptomycin (Gibco) and maintained in 37ºC incubators with 5% CO_2.

566   Four days prior to measurement, 293T-Dual cells were passaged and plated in 12-well tissue cultured-

567   treated plates at 100000 cells/well. After 20 hours they were transfected with 100 ng of pcDNA3-

568   hSTING and 100 ng of pcDNA3 empty vector or containing Acb2 using Fugene6 transfection reagent

569   (Promega) according to its associated protocol. After 20 hours, the growth media was replaced with

570   fresh growth media containing 50 µM 2',3'-cGAMP or regular growth media as negative controls. The

571   cells were further incubated for 18 h, and the media was harvested to measure luciferase activity using

572   the QuantiLuc system (Invivogen). The cells were directly lysed in $1 \times$ LSB and western blot was

573   performed on cell lysates to verify expression of STING and Acb2.

574

575   **Western blot**

576   A rabbit Acb2 polyclonal antibody was generated by a commercial vender (GenScript) using a

577   synthetic peptide from Acb2 (CHNRDEITRIANAEP). The polyclonal Acb2 antibody was further

578   purified by antigen affinity (GenScript).

579

580   After harvesting conditioned media, cells were directly lysed on the plate using $1\times$ LSB. Lysates were

581   separated on a SurePage Bis-Tris polyacrylamide gel (GenScript) and transferred to a nitrocellulose

582   membrane using the semi-dry iBlot2 system (Invitrogen). The membrane was blocked for 1 h at room

583   temperature (Intercept blocking buffer, Li-COR Biosciences), and incubated with primary antibodies

584   (rabbit anti-STING (Cell Signaling Technologies), mouse anti-alpha-tubulin (Sigma-Aldrich), rabbit

585   anti-Acb2 (GenScript)) overnight at 4ºC. Following three washes in $1\times$TBS-0.1% tween, secondary

586   antibody (Anti-rabbit or anti-mouse (Li-Cor Biosciences)) was added for 1 hour at room temperature,

587   followed by three additional washes in TBS-T. Blots were imaged in IR using a Li-Cor Odyssey Blot

588   Imager.

589

References

Adams, P.D., Grosse-Kunstleve, R.W., Hung, L.W., Ioerger, T.R., and Terwilliger, T.C. (2002). PHENIX: building new software for automated crystallographic structure determination. Acta Crystallographica Section D Biological Crystallography *58*, 1948-1954.

Athukoralage, J.S., and White, M.F. (2022). Cyclic Nucleotide Signaling in Phage Defense and Counter-Defense. Annual review of virology *9*, 451-468.

Burdette, D.L., Monroe, K.M., Sotelo-Troha, K., Iwig, J.S., Eckert, B., Hyodo, M., Hayakawa, Y., and Vance, R.E. (2011). STING is a direct innate immune sensor of cyclic di-GMP. Nature *478*, 515-U111.

Burroughs, A.M., Zhang, D., Schäffer, D.E., Iyer, L.M., and Aravind, L. (2015). Comparative genomic analyses reveal a vast, novel network of nucleotide-centric systems in biological conflicts, immunity and signaling. Nucleic acids research *43*, 10633-10654.

Cady, K.C., Bondy-Denomy, J., Heussler, G.E., Davidson, A.R., and O'Toole, G.A. (2012). The CRISPR/Cas adaptive immune system of Pseudomonas aeruginosa mediates resistance to naturally occurring and engineered phages. J Bacteriol *194*, 5728-5738.

Cai, H., Li, L., Slavik, K., Huang, J., Yin, T., Hédelin, L., Xiang, Z., Yang, Y., Li, X., Chen, Y., *et al.* (2023). A novel virus-induced cyclic dinucleotide, 2′3′-c-di-GMP, mediates STING-dependent antiviral immunity in Drosophila. bioRxiv, 2023.2005.2008.539652.

Cohen, D., Melamed, S., Millman, A., Shulman, G., Oppenheimer-Shaanan, Y., Kacen, A., Doron, S., Amitai, G., and Sorek, R. (2019). Cyclic GMP-AMP signalling protects bacteria against viral infection. Nature *574*, 691-695.

Davies, B.W., Bogard, R.W., Young, T.S., and Mekalanos, J.J. (2012). Coordinated regulation of accessory genetic elements produces cyclic di-nucleotides for V. cholerae virulence. Cell *149*, 358-370.

Duncan-Lowey, B., McNamara-Bordewick, N.K., Tal, N., Sorek, R., and Kranzusch, P.J. (2021). Effector-mediated membrane disruption controls cell death in CBASS antiphage defense. Mol Cell *81*, 5039-5051.e5035.

Eaglesham, J.B., and Kranzusch, P.J. (2020). Conserved strategies for pathogen evasion of cGAS-STING immunity. Current opinion in immunology *66*, 27-34.

Emsley, P., Lohkamp, B., Scott, W., and Cowtan, K. (2010). Features and development of Coot. Acta Crystallogr *66*, 486-501

Fatma, S., Chakravarti, A., Zeng, X., and Huang, R.H. (2021). Molecular mechanisms of the CdnG-Cap5 antiphage defense system employing 3',2'-cGAMP as the second messenger. Nat Commun *12*, 6381.

Hobbs, S.J., Wein, T., Lu, A., Morehouse, B.R., Schnabel, J., Leavitt, A., Yirmiya, E., Sorek, R., and Kranzusch, P.J. (2022). Phage anti-CBASS and anti-Pycsar nucleases subvert bacterial immunity. Nature *605*, 522-526.

Holm, L. (2022). Dali server: structural unification of protein families. Nucleic acids research *50*,

627   W210-w215.

628   Huiting, E., Cao, X., Ren, J., Athukoralage, J.S., Luo, Z., Silas, S., An, N., Carion, H., Zhou, Y., Fraser,
629   J.S*., et al.* (2023). Bacteriophages inhibit and evade cGAS-like immune function in bacteria. Cell *186*,
630   864-876 e821.

631   Ishikawa, H., and Barber, G.N. (2008). STING is an endoplasmic reticulum adaptor that facilitates
632   innate immune signalling (vol 455, pg 674, 2008). Nature *456*, 274-274.

633   Jenson, J.M., Li, T., Du, F., Ea, C.K., and Chen, Z.J. (2023). Ubiquitin-like Conjugation by Bacterial
634   cGAS Enhances Anti-phage Defence. Nature *616*, 326-331.

635   Ko, T.P., Wang, Y.C., Yang, C.S., Hou, M.H., Chen, C.J., Chiu, Y.F., and Chen, Y. (2022). Crystal
636   structure and functional implication of bacterial STING. Nat Commun *13*, 26.

637   Lau, R.K., Ye, Q., Birkholz, E.A., Berg, K.R., Patel, L., Mathews, I.T., Watrous, J.D., Ego, K., Whiteley,
638   A.T., Lowey, B*., et al.* (2020). Structure and Mechanism of a Cyclic Trinucleotide-Activated Bacterial
639   Endonuclease Mediating Bacteriophage Immunity. Mol Cell *77*, 723-733 e726.

640   Leavitt, A., Yirmiya, E., Amitai, G., Lu, A., Garb, J., Herbst, E., Morehouse, B.R., Hobbs, S.J., Antine,
641   S.P., Sun, Z.-Y.J*., et al.* (2022). Viruses inhibit TIR gcADPR signaling to overcome bacterial defense.
642   Nature *611*, 326-331.

643   Li, X.D., Wu, J., Gao, D., Wang, H., Sun, L., and Chen, Z.J. (2013). Pivotal roles of cGAS-cGAMP
644   signaling in antiviral defense and immune adjuvant effects. Science *341*, 1390-1394.

645   Lowey, B., Whiteley, A.T., Keszei, A.F.A., Morehouse, B.R., Mathews, I.T., Antine, S.P., Cabrera, V.J.,
646   Kashin, D., Niemann, P., Jain, M*., et al.* (2020). CBASS Immunity Uses CARF-Related Effectors to
647   Sense 3'-5'- and 2'-5'-Linked Cyclic Oligonucleotide Signals and Protect Bacteria from Phage Infection.
648   Cell *182*, 38-49.e17.

649   Mayo-Muñoz, D., Smith, L.M., Garcia-Doval, C., Malone, L.M., Harding, K.R., Jackson, S.A.,
650   Hampton, H.G., Fagerlund, R.D., Gumy, L.F., and Fineran, P.C. (2022). Type III CRISPR-Cas provides
651   resistance against nucleus-forming jumbo phages via abortive infection. Mol Cell *82*, 4471-
652   4486.e4479.

653   Millman, A., Melamed, S., Amitai, G., and Sorek, R. (2020). Diversity and classification of cyclic-
654   oligonucleotide-based anti-phage signalling systems. Nature microbiology *5*, 1608-1615.

655   Molina, R., Sofos, N., and Montoya, G. (2020). Structural basis of CRISPR-Cas Type III prokaryotic
656   defence systems. Curr Opin Struct Biol *65*, 119-129.

657   Morehouse, B.R., Yip, M.C.J., Keszei, A.F.A., McNamara-Bordewick, N.K., Shao, S., and Kranzusch,
658   P.J. (2022). Cryo-EM structure of an active bacterial TIR-STING filament complex. Nature *608*, 803-
659   807.

660   Otwinowski, Z., and Minor, W. (1997). [20] Processing of X-ray diffraction data collected in oscillation
661   mode - ScienceDirect. Methods in Enzymology *276*, 307-326.

662   Qiu, D., Damron, F.H., Mima, T., Schweizer, H.P., and Yu, H.D. (2008). PBAD-based shuttle vectors
663   for functional analysis of toxic and highly regulated genes in Pseudomonas and Burkholderia spp. and

664   other bacteria. Appl Environ Microbiol *74*, 7422-7426.

665   Slavik, K.M., Morehouse, B.R., Ragucci, A.E., Zhou, W., Ai, X., Chen, Y., Li, L., Wei, Z., Bähre, H.,
666   König, M.*, et al.* (2021). cGAS-like receptors sense RNA and control 3'2'-cGAMP signalling in
667   Drosophila. Nature *597*, 109-113.

668   Tal, N., Morehouse, B.R., Millman, A., Stokar-Avihail, A., Avraham, C., Fedorenko, T., Yirmiya, E.,
669   Herbst, E., Brandis, A., Mehlman, T.*, et al.* (2021). Cyclic CMP and cyclic UMP mediate bacterial
670   immunity against phages. Cell *184*, 5728-5739 e5716.

671   van Beljouw, S.P.B., Sanders, J., Rodriguez-Molina, A., and Brouns, S.J.J. (2022). RNA-targeting
672   CRISPR-Cas systems. Nat Rev Microbiol *21*, 21-34.

673   van Kempen, M., Kim, S.S., Tumescheit, C., Mirdita, M., Lee, J., Gilchrist, C.L.M., Söding, J., and
674   Steinegger, M. (2023). Fast and accurate protein structure search with Foldseek. Nature biotechnology.
675   doi: 10.1038/s41587-023-01773-0

676   Whiteley, A.T., Eaglesham, J.B., de Oliveira Mann, C.C., Morehouse, B.R., Lowey, B., Nieminen,
677   E.A., Danilchanka, O., King, D.S., Lee, A.S.Y., Mekalanos, J.J.*, et al.* (2019). Bacterial cGAS-like
678   enzymes synthesize diverse nucleotide signals. Nature *567*, 194-199.

679   Woodward, J.J., Iavarone, A.T., and Portnoy, D.A. (2010). c-di-AMP secreted by intracellular Listeria
680   monocytogenes activates a host type I interferon response. Science *328*, 1703-1705.

681   Ye, Q., Lau, R.K., Mathews, I.T., Birkholz, E.A., Watrous, J.D., Azimi, C.S., Pogliano, J., Jain, M.,
682   and Corbett, K.D. (2020). HORMA Domain Proteins and a Trip13-like ATPase Regulate Bacterial
683   cGAS-like Enzymes to Mediate Bacteriophage Immunity. Mol Cell *77*, 709-722.e707.

684   Yirmiya, E., Leavitt, A., Lu, A., Avraham, C., Osterman, I., Garb, J., Antine, S.P., Mooney, S.E., Hobbs,
685   S.J., Kranzusch, P.J.*, et al.* (2023). Phages overcome bacterial immunity via diverse anti-defense
686   proteins. bioRxiv, 2023.2005.2001.538930.